Hybrid Navigation for Launchers Using Multiple Low-Cost Inertial Measurement Units

Tiago Milhano [(1)], Dimitrios Gkoutzos [(1)], Julia Gente [(1)]

[(1)] Astos Solutions GmbH, Meitnerstrasse 8, 70563 Stuttgart Germany, phone: +49 711 892633 - 27, emails: tiago.milhano@astos.de, dimitrios.gkoutzos@astos.de, julia.gente@astos.de

ABSTRACT

This paper proposes an architecture for a multiple IMU hybrid navigation system for launch vehicles based on a Federated Filter Fusion scheme. A master filter fuses the several local navigation solutions of GNSS-aided inertial navigation systems, one for each IMU. The local filters are comprised of strapdown inertial propagation algorithms and error-state Schmidt-Kalman filters for GNSS measurement integration. The master filter fuses the outputs of the federated filters based on the individually estimated covariances, being a least squares estimator. An averaged calibrated measurement of angular rate and specific force acceleration is also provided by the fusion filter. The performance of the developed navigation scheme with 2-5 low-grade IMUs is compared with the results obtained with a single low- and a single medium-grade units. A comparison between the results obtained with a cluster of 4 IMUs at the top of the launcher and with a set of 4 distributed units, two at the top of the launcher and two that are jettisoned with the 1st and 2nd stages, is also presented. The sensor data is simulated on a realistic micro launcher scenario using ASTOS, being subjected to angle and velocity random walk, bias, bias instability, scale factor and misalignment.

1 INTRODUCTION

The NewSpace landscape for micro launchers is highly competitive with the cost being one of the decisive factors in this competition. Several micro launcher companies have decided to outsource the GNC sub-system development to external providers, procuring low-cost commercial-of-the-shelf solutions. Astos Solutions has been involved in several activities related to the development of GNC software and tools for (micro)launchers to meet this increasing demand. With a customer base of 40+ micro launcher companies, Astos' lately established GNC department has been focused on providing GNC development tools and flexible and easily reconfigurable GNC software that can be applied to a wide range of launch vehicles.

Navigation is one of the main drivers for launcher orbital injection accuracy and it is also one of the main drivers for cost in the GNC sub-system. Usually, this cost is driven by the Inertial Navigation System (INS) or Inertial Measurement Unit (IMU), in which expensive technologies are employed such as ring-laser gyroscopes. In traditional inertial propagation algorithms, errors are accumulated due to integration resulting in a steady divergence of the position and attitude estimate. Therefore, the performance of the navigation mainly depends on the performance of the IMU. This makes an investment into highly accurate inertial sensors, especially the gyroscope, necessary to meet the navigation requirements. Lately, the use of hybrid navigation solutions that fuse the inertial measurements with Global Navigation Satellite Systems (GNSS) measurements has diminished, in

some degree, the reliance of the navigation algorithm on the IMU performance ([1], [3], [4]). Although this is true for translational states, as position and velocity, the same cannot be said with the same degree of validity for attitude determination and, more specifically, for roll angle estimation.

One possible way to reduce the cost of inertial sensors is by using microelectromechanical systems (MEMS). The advantages of using this technology, apart from the large reduction in cost, are the significant saves in mass and power required to operate these sensors. The disadvantage is clearly the lower performance, especially in high-vibration environments such as encountered in launcher vehicles. Lately, efforts to improve the performance of MEMS navigation solutions were driven by the demand of industries such as the wearables and unmanned aerial systems. This led to the development of solutions that utilize multiple low-cost inertial measurement units ([5], [6]). Also, multiple IMU navigation architectures have been proposed for launch vehicles, using augmented and stacked filters [7]. By using multiple IMU, the hardware cost is not gravely increased in exchange for higher navigation accuracy, reliability, and redundancy.

In this paper, a navigation algorithm is proposed that incorporates the measurements from multiple IMUs, based on the Federated Filter Fusion method. Each local filter implements a loosely coupled, closed-loop GNSS-aided inertial navigation system (INS), one for each IMU. The navigation solution, providing estimates of position, velocity, and attitude, is then a combination of the individual INS results through weighted means based on the covariance of the individual estimates.

An analysis will be presented relating the performance of the navigation architecture with the number of sensors used and their distribution on the launch vehicle's body. The resulting performances are compared to two baseline navigation solutions employing a single low- and medium-grade IMU. The simulated measurements used in the performance assessment are retrieved from high-fidelity 6 degrees-of-freedom non-linear simulator of a representative micro launcher scenario. The simulators' dynamics, kinematics, environment, and sensor modelling are provided by the ASTOS tool [1].

2 MULTIPLE IMU HYBRID NAVIGATION ARCHITECTURE

The proposed architecture for a multiple IMU hybrid navigation system is based on the Federated Filter Fusion method. Federated filtering consists of using decentralized filter scheme formed of local (or "*federated*") and master filters. The local filters feed their estimates of the state vector to the master filter, which, in turn, is responsible for fusing the estimates of the local filters. In the present study, the information flows in a single direction, from local to master filters, with no feedback from master to local filters. This configures a no reset information flow. The proposed navigation architecture is provided in Figure 1.

For the proposed solution, each local filter is formed of a GNSS-aided inertial navigation system. Each INS processes the measurement of a single IMU and updates the inertially propagated state estimates with the GNSS measurements. A single GNSS receiver is considered in this study, sharing the same position and velocity measurements with all the local filters, as detailed in Figure 1. The federated filter estimates the kinematic states of the launch vehicle, plus any states related to the sensors, such as calibration parameters, deemed necessary. Each federated filter is comprised of: (1) a strapdown inertial propagation (SIP) algorithm with gyro and accelerometer calibration models, described in section 2.1, which are executed at the IMU sampling frequency; and, (2) an error-state Schmidt-Kalman filter (eSKF), described in section 2.2, which is executed at the GNSS sampling frequency (except for the covariance propagation step which is executed at the same frequency as the SIP). The IMU calibration models are regularly corrected with the results of the fusion between SIP

and GNSS measurements, resulting in loosely coupled, closed-loop implementation of INS/GNSS integration.

The master filter shares the kinematic states of the launcher with the federated filters, but not the IMU sensor states. The later are still used by the master filter, as described in section 2.3, but are not modified by it. The kinematic states are fused using a weighted average using the estimated covariances provided by the local filters, i.e., the master filter is a least squares estimator.

This design of multiple IMU hybrid navigation architecture was selected due to its modularity and flexibility. The design allows to use any number of IMU with virtually no modifications. Additionally, each GNSS-aided INS local filter can be configured individually, tailored to the sensors feeding it with their measurements. Different tuning and even different sensor states can be used locally.

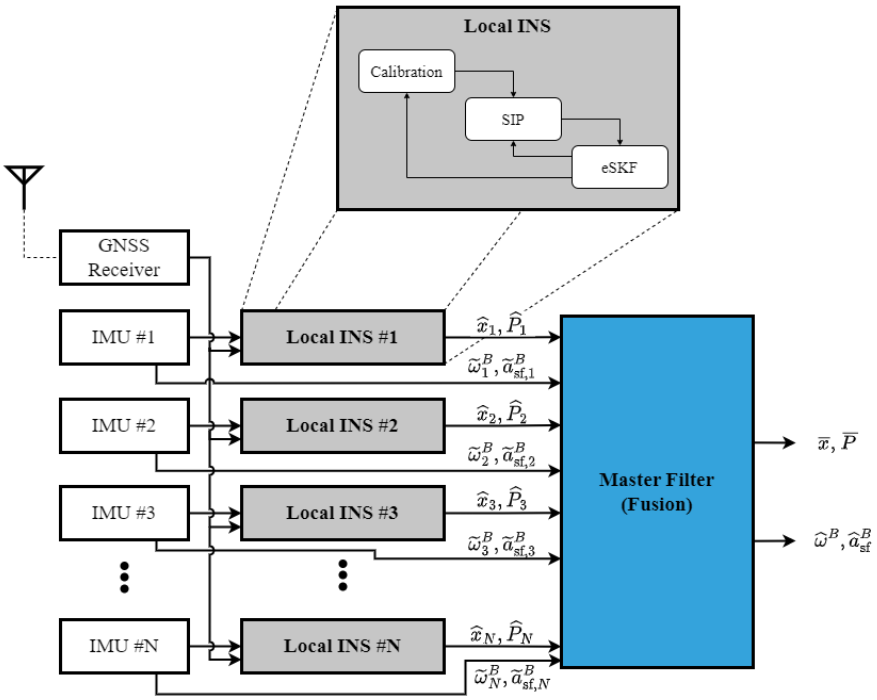

Figure 1: Multiple IMU hybrid navigation architecture

2.1 Local Strapdown Inertial Propagation

The strapdown inertial propagation of inertial measurements is used to provide a navigation solution. In this process, the IMU provides measurements such as angular rate ($\boldsymbol{\omega}_{IB}^{B}$) and specific-force acceleration ($\boldsymbol{a}_{sf}^{B}$) in the body-fixed frame, denoted as B. These measurements are obtained at a constant rate.

The attitude propagation is performed using attitude quaternions, as shown in (1), where $\Delta t\widehat{\omega}_{IB,k}^{B}$ is an approximation, through the Euler integration method, of the rotation angle between the body-fixed frame at the two time instants, where $\Delta t = t_{k+1} - t_k$ and $\widehat{\omega}_{IB,k}^{B} = \left\|\widehat{\boldsymbol{\omega}}_{IB,k}^{B}\right\|$.

$$\left\{\boldsymbol{q}_{I}^{B_{k+1}}\right\}^{(-)} = \boldsymbol{q}_{B_k}^{B_{k+1}}\left\{\boldsymbol{q}_{I}^{B_k}\right\}^{(+)}, \qquad \boldsymbol{q}_{B_k}^{B_{k+1}} \approx \begin{bmatrix} \cos\left(\frac{\Delta t}{2}\cdot\widehat{\omega}_{k}^{B}\right) \\ \frac{\widehat{\boldsymbol{\omega}}_{k}^{B}}{\widehat{\omega}_{k}^{B}}\sin\left(\frac{\Delta t}{2}\cdot\widehat{\omega}_{k}^{B}\right) \end{bmatrix} \tag{1}$$

where $\widehat{\boldsymbol{\omega}}_k^B$ is the short notation for $\widehat{\boldsymbol{\omega}}_{IB,k}^B$.

The propagation of the velocity and position are derived as in [8], albeit being expressed in inertial frame. It is assumed that the specific force acceleration is expressed in the coordinates of the body-fixed frame at the half the integration interval. Also, the gravitational acceleration is evaluated at the intermediate estimated position, i.e., the position at time $t_{k+1/2}$.
The gravitational acceleration is obtained recurring to a second-order gravitational model as in [9].
The calibration scheme is based on the ones presented in [2] and [8].

2.2 Local inertial/GNSS integration filter

The local filters are formulated as error-state Schmidt-Kalman filters (see [2], [8]). Then, the error-state models, $\delta\boldsymbol{x}_k = \boldsymbol{x}_k - \widehat{\boldsymbol{x}}_k$, can be written considering the contribution of the called consider-states, $\boldsymbol{c}$, which contain all the uncertain parameters that are set to their best-known values and are not to be estimated. The error-state model is expressed as

$$\delta\boldsymbol{x}_{k+1} = \phi(\widehat{\boldsymbol{x}}_k + \delta\boldsymbol{x}_k, \boldsymbol{c}) - \phi(\widehat{\boldsymbol{x}}_k, \boldsymbol{c}) + \boldsymbol{w}_{x,k} \tag{2}$$

which, linearized around the origin, yields

$$\delta\boldsymbol{x}_{k+1} = \boldsymbol{\Phi}_{xx,k}\delta\boldsymbol{x}_k + \boldsymbol{\Phi}_{xc,k}\boldsymbol{c} + \boldsymbol{w}_{x,k} \tag{3}$$

with the matrices

$$\boldsymbol{\Phi}_{xx,k} = \left.\frac{\partial\phi(\boldsymbol{x}_k, \boldsymbol{c})}{\partial\boldsymbol{x}_k}\right|_{\widehat{\boldsymbol{x}}_k, \widehat{\boldsymbol{c}}}, \qquad \boldsymbol{\Phi}_{xc,k} = \left.\frac{\partial\phi(\boldsymbol{x}_k, \boldsymbol{c})}{\partial\boldsymbol{c}}\right|_{\widehat{\boldsymbol{x}}_k, \widehat{\boldsymbol{c}}}. \tag{4}$$

and $\boldsymbol{w}_{x,k} \sim \mathcal{N}(\boldsymbol{0}, Q_k)$.

The estimated filter whole-states and error-states are

$$\widehat{\boldsymbol{x}}_k = \begin{bmatrix} \widehat{\boldsymbol{q}}_{B_k}^I & \widehat{\boldsymbol{v}}_k^I & \widehat{\boldsymbol{r}}_k^I & \widehat{\boldsymbol{\beta}}_{g,k} & \widehat{\boldsymbol{\beta}}_{a,k} \end{bmatrix}^T \tag{5}$$

$$\delta\widehat{\boldsymbol{x}}_k = \begin{bmatrix} \delta\boldsymbol{\psi}_k^B & \delta\widehat{\boldsymbol{v}}_k^I & \delta\widehat{\boldsymbol{r}}_k^I & \delta\widehat{\boldsymbol{\beta}}_{g,k} & \delta\widehat{\boldsymbol{\beta}}_{a,k} \end{bmatrix}^T. \tag{6}$$

In order in Eq. (5), one has the attitude quaternion from body-fixed to inertial frame, velocity and position in inertial frame, and the gyroscope and accelerometer biases. The first element of the error-state represents the three-axis angular error represented in body-fixed frame.

The set of consider parameters is

$$\hat{\boldsymbol{c}} = \begin{bmatrix} \hat{\boldsymbol{\lambda}}_g & \widehat{\boldsymbol{\mu}}_g & \hat{\boldsymbol{\lambda}}_a & \widehat{\boldsymbol{\mu}}_a & \widehat{\boldsymbol{\beta}}_R \end{bmatrix}^T \tag{7}$$

where, from left to right, one has the gyro scale factor and misalignment vectors, the accelerometer scale factor and misalignment vectors, and a GNSS position measurement bias. The uncertainty of these parameters is represented by the covariance matrix

$$P_{cc} = E[(\boldsymbol{c} - \hat{\boldsymbol{c}})(\boldsymbol{c} - \hat{\boldsymbol{c}})^T] \tag{8}$$

By executing the SIP at successive time steps, the error covariance typically increases. In this case, the increase in the uncertainty in the error-states estimates is driven by the process noise covariance,

Q_k, and the covariance of the consider-states, P_{cc}. If whole-state estimate has not yet been updated with the error-state estimate and the latter reset, the error-state estimate can be propagated as in Eq. (3).

The innovation vector is defined as

$$\boldsymbol{z}_{k+1} = \delta\boldsymbol{y}_{k+1} - h\left(\hat{\boldsymbol{x}}_{k+1}^{(-)} + \delta\hat{\boldsymbol{x}}_{k+1}^{(-)}, \hat{\boldsymbol{c}}\right) + h\left(\hat{\boldsymbol{x}}_{k+1}^{(-)}, \hat{\boldsymbol{c}}\right) \tag{9}$$

where $\delta\boldsymbol{y}_{k+1} = \tilde{\boldsymbol{y}}_{k+1} - h\left(\hat{\boldsymbol{x}}_{k+1}^{(-)}, \hat{\boldsymbol{c}}\right)$ is the error measurement vector, and h is the measurement model function. Eq. (9) then results in

$$\boldsymbol{z}_{k+1} = \tilde{\boldsymbol{y}}_{k+1} - h\left(\hat{\boldsymbol{x}}_{k+1}^{(-)} + \delta\hat{\boldsymbol{x}}_{k+1}^{(-)}, \hat{\boldsymbol{c}}\right). \tag{10}$$

When an updated estimate of the error-state is available, the whole-state estimate is updated, and the error-state estimate is reset:

$$\begin{gathered}\hat{\boldsymbol{x}}_{k+1}^{(+)} = \hat{\boldsymbol{x}}_{k+1}^{(-)} + \delta\hat{\boldsymbol{x}}_{k+1}^{(+)}, \\ \delta\hat{\boldsymbol{x}}_{k+1}^{(+)} \leftarrow 0\end{gathered} \tag{11}$$

The uncertainty of the state estimates with respect to itself and with respect to the consider-parameters are also updated.

Regarding the work presented in this paper, the measurement vector for a loosely coupled hybrid navigation algorithm is formed by the GNSS measured position and velocity, expressed in an Earth-fixed frame (denominated by the superscript E):

$$\boldsymbol{y}_k = \begin{bmatrix}\tilde{\boldsymbol{r}}_k^E \\ \tilde{\boldsymbol{v}}_k^E\end{bmatrix}. \tag{12}$$

Since, for the selected scenario, a launch-pad phase is included, during this stage the position and velocity measurements of the GNSS receiver are replaced by pseudo-measurements of the GNSS antenna on the launch pad position and zero velocity. Additionally, a third measurement vector is introduced with a pseudo-measurement of the Earth's angular rate.

2.3 Fusion of Federated Filters

The federated filters and the master filter share the launch vehicle kinematic states, although, in the current implementation of the proposed navigation architecture, each filter is estimating the position, velocity, and attitude of each IMU. Therefore, the first step of the fusion process is to express each filter's position and velocity estimates in a common point on the launch vehicle's body. The common reference point selected for this implementation is the GNSS antenna phase centre. It is assumed, at navigation level, a rigid launcher and, without loss of generality and for the sake of simplicity, it is considered that all the IMUs are aligned with body-fixed frame. Since all IMUs are aligned, no previous conversion is required for the angular rates and attitude estimates.

The inertial position and velocity estimates of the n^{th} IMU, $\boldsymbol{r}_{n,k}^F$ and $\boldsymbol{v}_{n,k}^F$, are expressed in the fusion reference point (denoted by superscript F). The averaged calibrated angular rate is obtained from the calibrated measurements of each individual IMU. Additionally, an averaged calibrated acceleration for the reference point is also provided by the federated fusion process. The individual calibrated acceleration signals are transformed to the reference point using the Grubin transformation. Then, the fused estimates and their covariance are calculated as

$$\bar{\boldsymbol{x}}_k = \begin{bmatrix} \bar{\boldsymbol{\theta}}^I_{B,k} \\ \bar{\boldsymbol{v}}^F_k \\ \bar{\boldsymbol{r}}^F_k \end{bmatrix} = \bar{P}_k \left(\sum_{n=1}^{N_{IMU}} P^{-1}_{n,k} \boldsymbol{x}^F_{n,k} \right) \tag{13}$$

$$\bar{P}_k = \sum_{n=1}^{N_{IMU}} P^{-1}_{n,k}, \qquad \boldsymbol{x}^F_{n,k} = \begin{bmatrix} \boldsymbol{\theta}^I_{B_n,k} \\ \boldsymbol{v}^F_{n,k} \\ \boldsymbol{r}^F_{n,k} \end{bmatrix} \tag{14}$$

where $P_{n,k}$ is the covariance estimate of the n^{th} filter for the kinematic states, i.e., it is a 9-by-9 truncation of the estimated covariance matrix, and $\boldsymbol{\theta}^I_{B_n,k}$ is the attitude estimate of the n^{th} filter represented in Euler angles.

3 PERFORMANCE ASSESSMENT

In this section, the proposed hybrid navigation scheme performance is assessed. The data for the performance tests was obtained for a scenario comprising of three-stage micro launcher vehicle targeting 500km of altitude Sun-Synchronous Orbit (SSO). The vehicle first targets an elliptical transfer orbit with its three stages and coasts, before performing a circularization burn with the Attitude and Orbit Control System (AOCS) thrusters into the desired SSO. The mission timeline can be seen in Table 1. All the dynamics, kinematics, environment, actuator, and sensor models are emulated by ASTOS [1], running in Simulink. A single trajectory is used, however 200 realizations of the GNSS receiver and each IMU measurement errors are produced to perform Monte Carlo (MC) tests. These tests are executed offline.

Table 1: Mission Timeline

Flight Time (app.) [s]	Event
0	Launch Pad
600	Lift Off - First Stage Burning
710	Coasting Phase
730	Second Stage Burning
839.9	Third Stage Burning
958.7	Coasting to Apogee
2715	Circularization Burn
2940	End

First, a baseline performance is established using a single IMU architecture. The results are obtained using two different grade levels of IMU: a medium- and a low-grade unit. Secondly, the navigation results of fusing the estimates of multiple IMUs using the federated filter architecture are presented. For this last set of tests, results will be presented from 2 and up to 5 IMU, with all of them positioned at the top of the third stage. Finally, the results of having the 4 units placed at the top of the third stage will be compared with the results of 2 sensors placed at the top of the 3rd stage and 2 more located at the top of the 1st and 2nd stages. Two of the sensors will be lost as the flight progresses, ejected together with their respective stages.

The placement of the sensors mounted at the top of the 3rd stage, located 24m from the first stage engine mounting point, can be seen in Figure 2. They are placed in a ring with a 90cm radius (units R1 to R4), and one placed in the longitudinal axis (unit REF). Additionally, two more IMU are considered. They are mounted along the longitudinal axis of the launcher at the top of the first and second stage (12 and 20m from the base of the 1st stage), denominated L1 and L2, respectively. The GNSS receiver antenna phase centre is located at the same location as the measurement unit REF.

The sensor error modelling parameters (1-σ values) used in the presented work are given in Table 2. The values for the inertial measurement units are retrieved from [2] and, as stated there, they are representative of the current European state-of-the-art in inertial sensors. The medium-grade parameters are based on typical values for fiber optic or hemispherical resonating gyros, while the low-grade parameters are typical of MEMS technology inertial units. The error sources used in the tests are, for both accelerometers and gyros: velocity (angle) random walk noise, bias initialization error, bias instability, scale factor, and misalignment. The IMU sampling frequency is 100Hz. The GNSS receiver position error is modelled as a constant plus white-noise and the velocity is perturbed by white-noise. The GNSS measurements are provided at 1Hz. The parameter values are also reported in Table 2.

Table 2: Sensor error source values considered in this study.

Parameter	Unit	Low	Medium
Gyro Performance (1-σ values)			
Angle RW (ARW)	$\mathrm{deg}/\sqrt{\mathrm{h}}$	0.15	0.01
Bias initialization	deg/h	1	0.1
Bias instability, 1h	deg/h	1	0.3
Scale factor (on/off)	ppm	1000	400
Misalignment	μrad	1000	300
Accelerometer Performance (1-σ values)			
Velocity RW (VRW)	$\mu\mathrm{g}/\sqrt{\mathrm{Hz}}$	10000	1000
Bias initialization	μg	2000	500
Bias instability	μg	1500	50
Scale factor (on/off)	ppm	400	200
Misalignment	μrad	1000	300
GNSS Receiver Performance			
Position bias (constant)	m	$\mathcal{U}(-10,10)$	
Position noise	m	$\mathcal{N}(0,5)$	
Velocity noise	m/s	$\mathcal{N}(0,0.2)$	

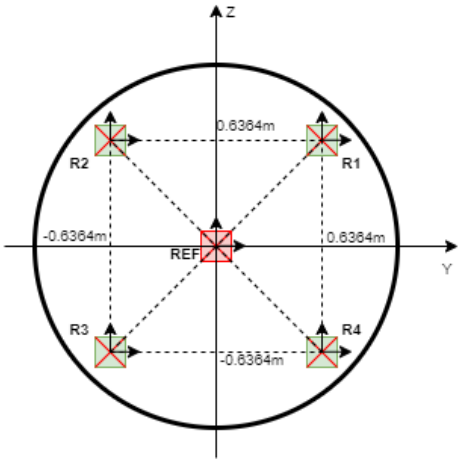

Figure 2: Placement of the IMUs Ref and R1-R4

3.1 Baseline with single IMU solution

A comparison is made between the results obtained with the filter described in section 2 using a single low- or medium-grade IMU. The IMU are placed in REF (see Figure 2).

The position error for one simulation of each grade of unit is shown in Figure 3 (a). The error is not much different between the two simulations. Similar results were expected since the position estimation quality is mainly driven by the GNSS receiver performance. Since the same receiver model is used on all simulations, the performance of the translational states will not differ much. It can be also seen that the standard deviation of the position estimated by the navigation filter is able to capture the uncertainty related to GNSS position measurement biases, due to their inclusion as consider parameters. The estimated standard deviation is very similar for the two filters and only a single line was plotted. Although the velocity performance is also related to the GNSS receiver performance, in this case there is a larger influence of the inertial propagation. This is clearly seen in the comparison between the velocity error for one simulation of each grade of unit presented in Figure 3 (b). When using the medium-grade IMU, a 3-fold improvement is observed.

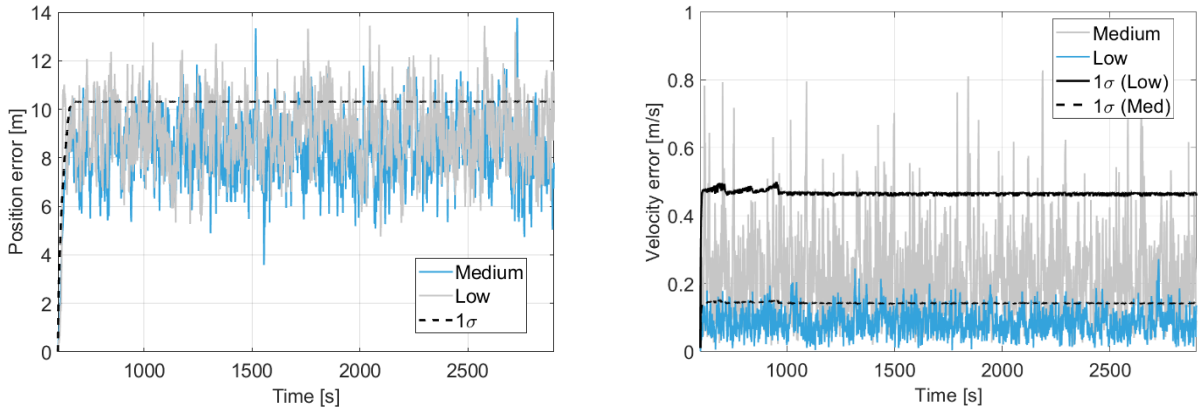

(a) (b)

Figure 3: Position and velocity error for both IMU grades and 1σ bounds in black.

The difference between employing a low- or medium-performance IMU becomes much more evident when analysing the attitude estimation errors. The attitude estimate error with the medium-grade IMU is presented in Figure 4 (a) for the 200 MC runs, with the dashed line showing the numerical 2σ bound, i.e., as computed from the MC results. The four main phases of the mission are clearly seen in the results. During the launch pad phase, the variance is kept low due to Earth rate pseudo-measurements, with error increasing slightly during the propelled flight phase, still with a 2σ around 0.05deg. Whilst coasting, the inexistence of a measured specific force acceleration causes the attitude error to increase. The GNSS measurements do not provide enough information to properly estimate the attitude. The errors in the gyros biases estimates are propagated together with the actual angular rate measurements leading to a linear increase in the propagated attitude error. The 2σ uncertainty increases at a rate of 0.24deg/h. Finally, during the circularization burn, apart from the oscillatory behaviour observed due to the ignition of the AOCS thrusters, the attitude uncertainty does not decrease. However, it seems to stabilize, finishing the circularization with a standard deviation of 0.0966 degrees.

The attitude estimate error with the low-grade IMU is presented in Figure 4 (b) for the 200 MC runs, similarly with the dashed line showing the numerical 2σ bound. The same phases are visible in the attitude error realizations. The uncertainty in attitude error 2σ bound remains approximately constant around 0.37deg. At the ignition of the first stage, 600s into the simulation, there is a spike in the error that reaches a maximum of 1.1deg over all runs. Then, the filter recovers slightly in the presence of a more dynamical regime, with the 2σ value varying between 0.26 and 0.28deg until the 3rd engine shutdown (at approximately second 960 of the simulation). The same linear trend is observed during coasting, as it was the case for the medium-grade results, with the 2σ uncertainty increasing at a rate of approximately 1.7deg/h. Even during the circularization burn, the attitude error increases as a trend, i.e., even disregarding the errors at the ignition of the AOCS thrusters, albeit at a lower rate. The reason for the attitude error increase, even when there is a specific force acceleration, is due to the very low thrust at which the circularization burn is performed in the considered scenario. The standard deviation of the attitude error at the end of circularization, for the hybrid navigation algorithm with the low-performance IMU, is 0.5957deg. A value 6 times worse than the one obtained with the medium-performance unit.

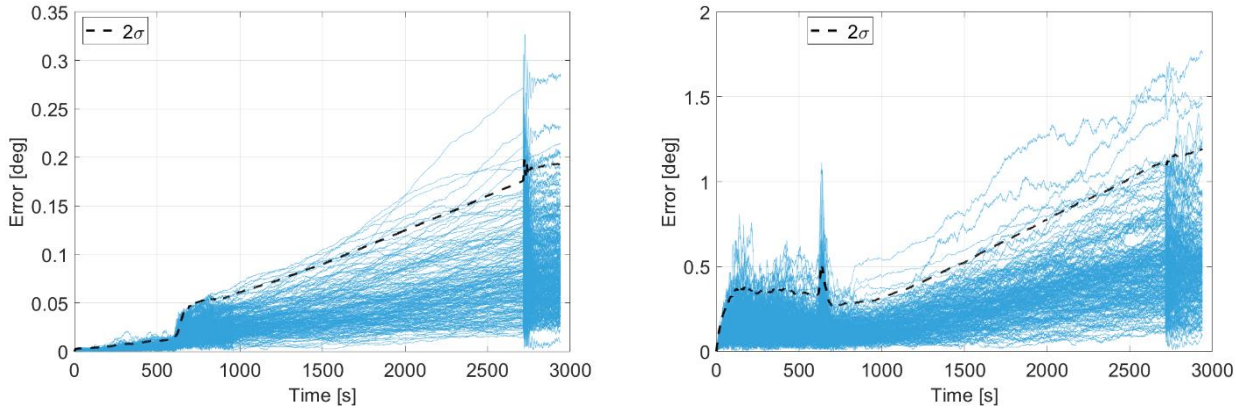

(a) (b)

Figure 4: Total attitude error for medium- (a) and low-grade (b) IMUs and 2σ bounds in black.

3.2 Multiple IMU fusion

This section shall focus on the hybrid navigation scheme performance presented in section 2 using multiple IMUs. The results of the different tests shall be compared in terms of the numerical standard deviation calculated from the MC results. The IMUs being used for each test are: R1 and R3; REF, R3 and R4; R1 to R4 and REF plus R1 to R4; when 2, 3, 4 and 5 units are used, respectively.

A comparison between the standard deviation of the total attitude error during the launch vehicle mission is presented in Figure 5 (a). Results are presented for the multiple IMU test results as well as the single unit results, both low- and medium-grade. As expected, the results of the fusion of more than one low-performance units are better than the single low-grade IMU configuration and the improvement is higher the larger the number of local filter estimates fused. However, it can be observed that, as the number of units increases, the consecutive relative improvements get smaller. Figure 5 (b) shows the percentage of improvement with respect to the attitude error standard deviation of the results using a single low-performance IMU along the simulated mission for each multiple IMU configuration. At the end of the circularization burn, 36, 43, 52 and 56% improvement are achieved for the configurations with 2 to 5 units, respectively. The results are summarized in Table 3.

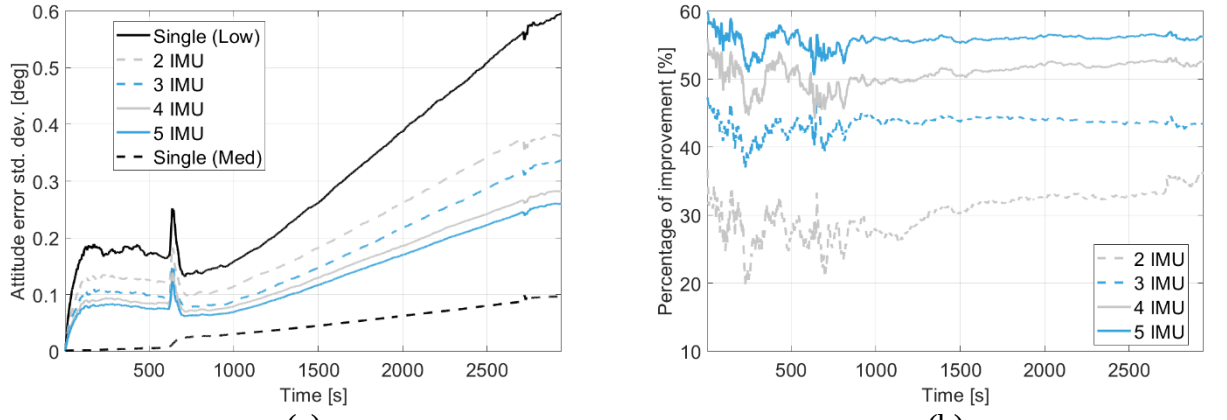

(a) (b)

Figure 5: Total attitude error standard deviation for the different tests (a); and the respective percentage of improvement of the multiple IMU tests with respect to the single low-grade IMU results (b).

Similar improvements can be seen in the estimated inertial velocity. The results are shown, from lift-off to the end of the circularization burn, in Figure 6. The same conclusions can be draw for the velocity results, as for the attitude ones: 1) the standard deviation of the error decreases as the number of low-grade units are used; 2) there are diminishing improvements as the number of units increases; and, 3) even when 5 low-performance units are employed, the fused navigation performance is still worse when compared with the results obtained with a single medium-grade IMU. The results are summarized in Table 3, where the mean standard deviation and relative improvement, from lift-off to the end of the circularization burn, are presented.

As mentioned in section 3.1, the position performance does not change in a significant manner independently of the number of IMUs used. The same reasons as presented in the previous section apply.

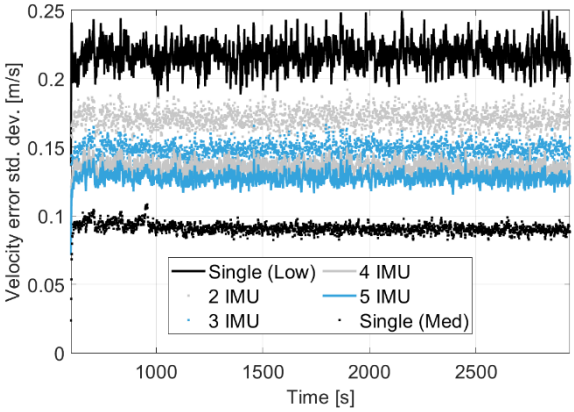

Figure 6: Velocity error standard deviation for the different test configurations.

The navigation function also provides calibrated measurements of angular rate and linear acceleration. These calibrated measurements result from the estimation of the measurement biases and, in the case of the configurations with multiple inertial measurement units, of the fusion of the different available measurements. Figure 7 shows the standard deviation of the calibrated measurements errors for: angular rate in (a) and for acceleration in (b). Again, apart from a small period of higher angular rate error at the beginning of circularization when the AOCS thrusters ignite, the same conclusions drawn for the attitude and velocity errors are applicable to the calibrated measurements. The results are summarized in Table 3, where the mean standard deviation and relative improvement are presented.

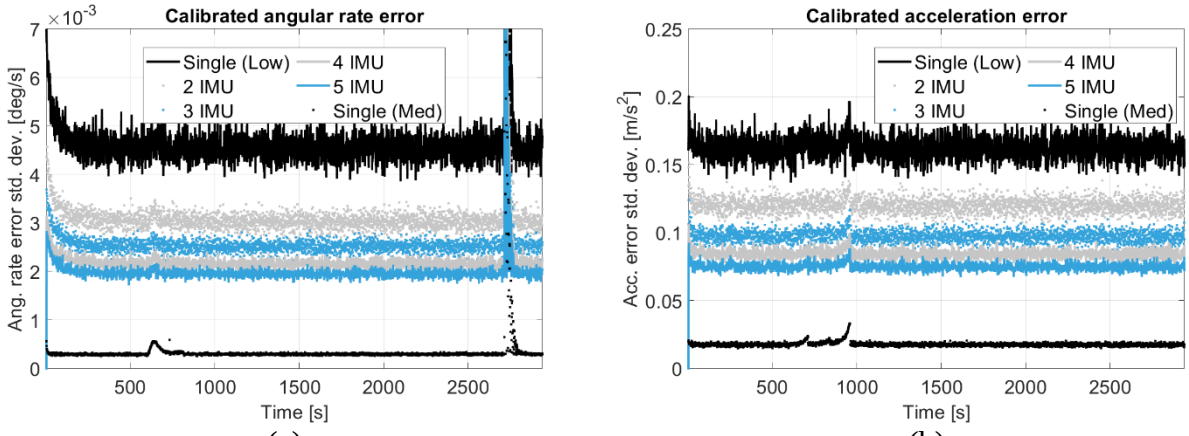

(a) (b)

Figure 7: Calibrated measurements errors for the different test configurations: (a) angular rate; and (b) acceleration.

Table 3: Summary of the results of the multiple tests

	Attitude (@end of circ.)		Velocity (mean)		Ang. Rate (mean)		Acceleration (mean)	
	1σ [deg]	imp. [%]	1σ [m/s]	imp. [%]	1σ [deg/s]	imp. [%]	1σ [m/s^2]	imp. [%]
Low	0.596	-	0.217	-	4.67e-3	-	0.162	-
2 IMU	0.380	36	0.171	22	3.14e-3	33	0.120	26
3 IMU	0.337	43	0.148	33	2.59e-3	44	0.0975	40
4 IMU	0.282	52	0.136	39	2.22e-3	52	0.0844	48
5 IMU	0.261	56	0.128	44	2.01e-3	57	0.0749	54
Medium	0.097	-	0.091	-	3.43e-4	-	0.0177	-

3.3 Clustered vs Distributed IMU Placement

This section attempts to evaluate the effects of having distributed units along the launch vehicle in opposition to having the same number clustered at the top of the 3rd stage. For that purpose, a MC test was conducted in which the units R1 and R3 are used together with units L1 and L2. The later are placed atop of the 1st and 2nd stages, respectively, and hence are jettisoned with their respective stage. This means that L2 IMU measurements are available during the three following phases: launch pad, 1st and 2nd stage burn, while the L1 unit measurements are available just during the first two.

The results are presented in Figure 8 and Figure 9, together with the results for the single low-grade IMU and for the tests with 2 and 4 clustered units. All the estimated quantities show the same trend: 1) equivalent performance to the 4 clustered unit configuration until the L1 unit is jettisoned together with the 1st stage; 2) equivalent performance to the 3 clustered unit configuration until the L2 unit is jettisoned together with the 2nd stage; and 3) equivalent performance to the 2 clustered unit configuration for the remaining simulation time. The only exception is the total attitude error at the launch pad. At this phase, the performance is closer to the one obtained with 2 units. This behaviour requires more investigation. However, the cause seems to be related to the calculation of the measurement sensitivity matrix used for the launch pad updates, namely the position and velocity derivates that are dependent on the lever-arm between each IMU and the GNSS antenna phase centre.

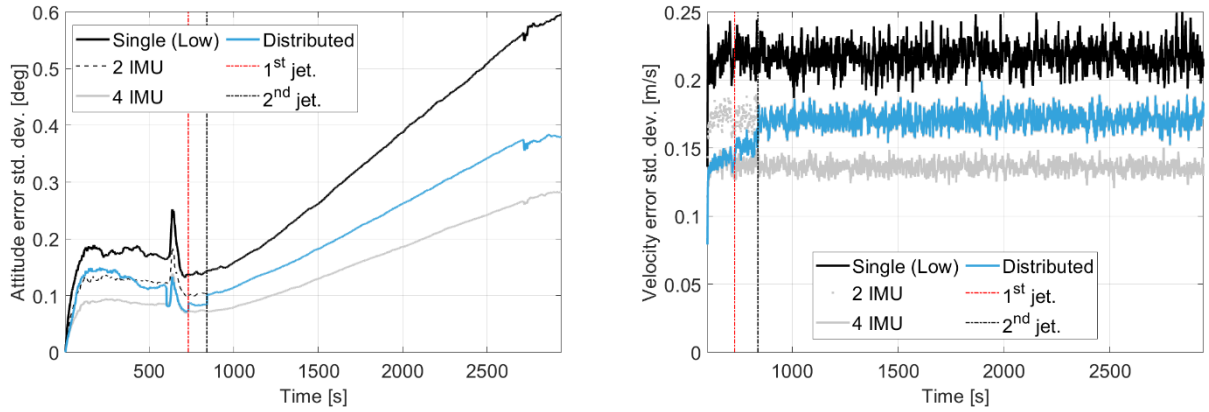

(a) (b)

Figure 8: Total attitude error (a) and velocity (b) standard deviation for the distributed test configuration

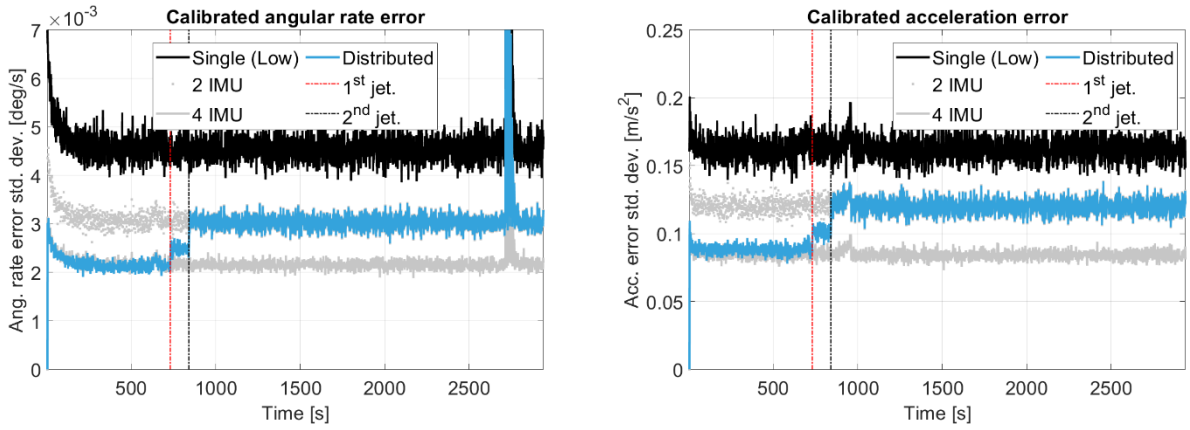

(a) (b)

Figure 9: Calibrated measurements errors for the distributed test configuration: (a) angular rate; and (b) acceleration.

4 CONCLUSIONS AND ROADMAP

A hybrid navigation architecture to incorporate measurements from multiple IMUs based on federated filter fusion has been proposed. A performance assessment analysis using simulated data from a micro launcher scenario has been presented. The performance of the proposed navigation scheme has been retrieved using two to five IMUs, clustered on the top of the third stage or distributed through all stages. The baseline for the performance assessment of the multiple units' tests were the results obtained using the same navigation algorithms present in the local filters for a single low- and medium-grade IMU. From the performance assessment of the tests performed with clustered IMUs, a summary of the main conclusions is as follows: (1) the standard deviation of the attitude and velocity error decreases as the number of units are used; (2) there are diminishing improvements as the number of units increases; (3) even when 5 low-performance units are employed, the attitude and velocity fused navigation estimate performance is still worse when compared with the results obtained with a single medium-grade IMU; and, (4) the performance of the position estimation is mainly driven by the GNSS receiver position measurement quality and no difference in estimation performance was observed over the different tests. The first 3 points presented previously also apply to the calibrated measurement of angular rate and acceleration provided by the fusion filter. Regarding the comparison of the results between clustered and distributed placements of the IMUs, the distributed placement strategy showed the same results as the clustered one, for the same number of units being used at a given time. No improvements were observed in pitch and yaw estimation. When 4 distributed units were being employed, prior to the first stage jettison, the estimation performance was equivalent to the one of 4 clustered units. After the first stage jettison, the performance of the distributed scheme degrades to the level of performance of 3 clustered units, with the same sequence happening after the second stage jettison.

Although the performances obtained using up to five low-performance IMUs did not reach the same level of performance while using a single medium-grade unit, it is the view of the authors that the proposed navigation architecture could still be of use in a plethora of scenarios. To provide some examples: the navigation requirements could fall within the range comprised between the performances obtained with a single low- and medium-grade IMUs and using multiple low-performance units still represent savings in cost, mass and power consumption; launch vehicles with multiple IMUs for redundancy could employ the proposed scheme to improve navigation accuracy without loss of said redundancy; and launch vehicles with actively recoverable first stages, that by design employ independent IMUs for controlled recovery of those stages, could make use of their

measurements during ascent for a better navigation accuracy and recoverable stage navigation initialization. Additionally, MEMS sensor technology has evolved quite significantly in recent years, closing the gap between what it is considered a low- and a medium-grade IMU.

The next steps in following the work presented in this study are to improve the fidelity of the simulated measurement generation and accordingly adapt and tune the local GNSS-aided INS filters; upgrade the algorithms implemented targeting real-time implementation, i.e., moving towards a embedded SW compatible implementation, and perform PIL testing; and, finally, perform tests with real flight data offline and, possibly onboard a sub-orbital rocket or micro launcher.

5 REFERENCES

[1] ASTOS: Analysis, Simulation and Trajectory Optimization Software for Space Applications. https://www.astos.de/products/astos

[2] Vandersteen J., Bennani S., and Roux C. "Robust Rocket Navigation with Sensor Uncertainties: Vega Launcher Application." *Journal of Spacecraft and Rockets* 55.1 (2018): 153-166.

[3] Trigo, G.F., et al. "Robust tightly coupled hybrid navigation for space transportation." *Journal of Spacecraft and Rockets* 56.2 (2019): 596-609.

[4] Steffes S. *Development and analysis of SHEFEX-2 hybrid navigation system experiment*. Diss. Bremen, Universität Bremen, Diss., 2013, 2013.

[5] Bancroft J.B., and Lachapelle G. "Data fusion algorithms for multiple inertial measurement units." *Sensors* 11.7 (2011): 6771-6798.

[6] Patel U.N. and Faruque I.A. "Multi-IMU Based Alternate Navigation Frameworks: Performance & Comparison for UAS." *IEEE Access* 10 (2022): 17565-17577.

[7] Beaudoin Y., et al. "Satellite launcher navigation with one versus three IMUs: Sensor positioning and data fusion model analysis." *Sensors* 18.6 (2018): 1872.

[8] Trigo G.F. *Low-Cost Failure-Tolerant Hybrid Navigation Designs for Future Space Transportation Systems*. Diss. Universität Bremen, 2020.

[9] Hough M.E. "Precise orbit determination using satellite radar ranging." *Journal of Guidance, Control, and Dynamics* 35.4 (2012): 1048-1058.